Acta Crystallographica Section B
Structural Science
ISSN 0108-7681

Structural refinements of high-pressure phases in germanium dioxide

Koichi Shiraki,[a]* Taku Tsuchiya[b] and Shigeaki Ono[c]

[a]Department of Earth Sciences, Kanazawa University, Kakuma-machi, Kanazawa-shi, Ishikawa 920-1165, Japan, [b]Department of Earth and Planetary Sciences, Tokyo Institute of Technology, 2-12-1 Ookayama, Meguro, Tokyo 152-8551, Japan, and [c]Institute for Frontier Research on Earth Evolution, Japan Marine Science and Technology Center, 2-15 Natsushima-cho, Yokosuka-shi, Kanagawa 237-0061, Japan

Correspondence e-mail: shiraki@earth.s.kanazawa-u.ac.jp

Received 23 March 2003
Accepted 30 September 2003

Recently, there has been substantial interest in the new high-pressure polymorphs of GeO_2 synthesized in the laboratory. Previous investigators reported the synthesis of '$CaCl_2$-type', 'α-PbO_2-type' and 'pyrite-type (modified-fluorite-type)' GeO_2 at pressures of 30–130 GPa in laser-heated diamond anvil cells. In order to provide definitive information about the new high-pressure polymorphs, we performed Rietveld refinements of the structures. The structure refinements confirm that two of these high-pressure phases do have the α-PbO_2-type and pyrite-type (modified-fluorite-type) structures.

1. Introduction

The transformation process of silica under pressure has been of long and continuing interest owing to its wide-ranging implications for geophysics, materials science and fundamental physics. Since the discovery of stishovite (rutile-type structure), a dense polymorph of silica with octahedrally coordinated silicon, there has been significant interest in the possibility of denser phases at high pressure. It has been shown that stishovite undergoes a displacive phase transformation to the $CaCl_2$-type structure at pressures above 50 GPa (Kingma *et al.*, 1995; Andrault *et al.*, 1998; Ono, Hirose, Murakami & Isshikik, 2002), in excellent agreement with first-principles predictions (Teter *et al.*, 1998; Karki *et al.*, 1997). In these predictions a similar theoretical sequence of phase transitions for silica was shown: rutile-type $\rightarrow$ $CaCl_2$-type $\rightarrow$ α-PbO_2-type $\rightarrow$ pyrite-type (modified fluorite-type). However, its behavior at higher pressures is not clear, as although new phases have been observed from both static and dynamic compression of amorphous silica (Liu *et al.*, 1978; Dubrovinsky *et al.*, 1997), α-cristobalite (Dubrovinsky *et al.*, 2001) and α-quartz (Kingma *et al.*, 1996; Haines *et al.*, 2001), the analysis of these data is difficult and contradictory. Several experimental studies at similar pressure and temperature conditions have yielded different results at similar pressure and temperature conditions. Hence, it is still unclear which phases of silica are stable at high pressure, which types of metastable phases are possible and which structural similarities may exist among them.

Among the dioxides (*e.g.* SiO_2, GeO_2, SnO_2, TiO_2, PbO_2, ZrO_2 and MnO_2), GeO_2 is the closest structural and low-pressure analog of SiO_2, as only SiO_2 and GeO_2 exhibit α-quartz-, rutile- and $CaCl_2$-type structures. Over the past three decades various physical and thermodynamical properties of rutile-type GeO_2 have been investigated: elastic properties (Liebermann, 1973), compressibility (Hazen & Finger, 1981),

Table 1
Experimental details of data collection and Rietveld analysis.

	$CaCl_2$-type	α-PbO_2-type	Pyrite-type
Data collection			
Crystal system	Orthorhombic	Orthorhombic	Cubic
Space group	*Pnnm*	*Pbcn*	$Pa\bar{3}$
Radiation type	Synchrotron	Synchrotron	Synchrotron
Wavelength (Å)	0.4133	0.4122	0.41295
Temperature (K)	300	2110	300
Pressure (GPa)	30.1	70.7	108.0
Refinement			
R_p	3.69	0.47	2.60
R_{wp}	6.77	0.77	3.80
R_{exp}	0.09	13.39	7.48
χ^2 (R_{wp}/R_{exp})	75.85	0.06	0.51
2θ range used (°)	6.012–17.208	7.004–16.390	8.001–14.999
2θ step width (°)	0.012	0.014	0.011
Preferred orientation parameter	0.99 (5)	No correction	No correction
Preferred orientation vector	{1 1 1}	–	–
No. of reflections used†	12	15	4
No. of parameters refined	28	34	31
No. of phase contained	2	3	3

$R_p = \Sigma w_i|y_i(\text{obs}) - y_i(\text{calc})|/\Sigma y_i(\text{calc})$. $R_{wp} = \{\Sigma w_i[y_i(\text{obs}) - y_i(\text{calc})]^2/\Sigma w_i[y_i(\text{calc})]^2\}^{1/2}$. χ^2 (goodness-of-fit) = $\Sigma w_i[y_i(\text{obs}) - y_i(\text{calc})]^2/(N_{obs} - N_{varpar})$. † Only for the phase of interest contained in each profile.

entropy and enthalpy (Navrotsky, 1971), thermal expansion (Rao *et al.*, 1968), structure (Baur & Khan, 1971) and melting phenomena (Jackson, 1976). However, high-pressure phases of GeO_2 have not been investigated. Recently, on the basis of high-temperature and high-pressure *in situ* X-ray experiments in a laser-heated diamond anvil cell (LHDAC), Ono *et al.* (2003*a*) demonstrated that $CaCl_2$-type GeO_2 transforms to an α-PbO_2-type phase at 40 GPa and to a pyrite-type (modified-fluorite-type) phase at higher pressures.

In this paper we confirm that the high-pressure phases are, in fact, $CaCl_2$-type, α-PbO_2-type and pyrite-type (modified-fluorite-type) phases, and report the results of a crystal structure refinement by means of the Rietveld method using selected X-ray diffraction profiles as described previously by Ono, Hirose, Nishiyama & Isshiki (2002) and Ono *et al.* (2003*a*,*b*).

2. Experimental

2.1. Data collection

Three X-ray diffraction profiles were selected to be analysed by Rietveld refinement. Such profiles which present a single phase of germanium dioxide were chosen in order to minimize any interference from reflections. The profile measurements were taken under high-pressure and temperature-quenched conditions for $CaCl_2$-type (300 K, 30.1 GPa; Ono, Hirose, Nishiyama & Isshiki, 2002) and pyrite-type GeO_2 (modified-fluorite-type; 300 K, 108 GPa; Ono *et al.*, 2003*b*). The $CaCl_2$-type sample was heated up to 2130 K, where the rutile-type phase occurred, and then quenched. The pyrite-type (modified-fluorite-type) sample was heated up to 2600 K. The data of the α-PbO_2-type structure were collected under high-pressure and high-temperature conditions (2110 K, 70.7 GPa; Ono *et al.*, 2003*a*). Hydrostatic pressure is expected to have been obtained by laser heating in the three samples during measurements.

High-pressure X-ray diffraction experiments were performed using the LHDAC high-pressure apparatus. Powdered α-quartz-type GeO_2 was used as the starting material. The starting material was loaded into holes drilled in rhenium gaskets. Platinum powder was mixed with the sample in order to absorb laser radiation for heating and to provide an internal pressure calibrant. The samples were heated with a multimode Nd:YAG laser (Ono, Hirose, Isshiki *et al.*, 2002) for *in situ* X-ray experiments, using double-sided laser heating techniques that minimize temperature gradients (both axial and radial) in the heated area (Shen *et al.*, 2001). The sample temperature was measured from one side of the sample using the spectroradiometric method. The spectroradiometric system consists of a thermoelectrically cooled CCD detector and a spectrograph. A pressure medium of NaCl was used, except for the pyrite-type (modified fluorite-type) phase.

The temperature-quenched samples of the $CaCl_2$- and pyrite-type (modified fluorite-type) phases, and the high-temperature sample of the α-PbO_2-type were probed by angle-dispersive X-ray diffraction using the synchrotron beamline BL10XU at SPring-8, a synchrotron radiation source at the Japan Synchrotron Radiation Research Institute (JASRI) in Japan. The conditions of data collection are listed in Table 1.[1] The incident X-ray beams were monochromated to wavelengths of *ca* 0.41 Å. The X-ray beam size was collimated to 20 µm diameter. The intensities observed on the imaging plates were integrated as a function of 2θ in order to obtain conventional, one-dimensional diffraction profiles. The pressure was determined from the observed unit-cell volume of platinum using the equation-of-state (EOS) for platinum given by Holmes *et al.* (1989), with an electronic thermal pressure correction (Tsuchiya & Kawamura, 2002).

Further experimental details can be obtained from Ono, Hirose, Nishiyama & Isshiki (2002) and Ono *et al.* (2003*a*,*b*).

2.2. Rietveld refinement

All three types of GeO_2 polymorph were refined using the atomic coordinates of *ab initio* calculations (Łodziana *et al.*, 2001) as the initial values. The program packages *RIETAN* (Izumi & Ikeda, 2000) and *VENUS* (Dilanian & Izumi, 2002) were used in this study for the Rietveld analysis and visuali-

[1] Supplementary data for this paper are available from the IUCr electronic archives (Reference: WS0004). Services for accessing these data are described at the back of the journal.

Table 2
Observed and calculated intensities and positions of the diffraction peaks for the $CaCl_2$-type structure.

Phase	*hkl*	2θ (°)	*d* (Å)	I_{obs}	I_{calc}
C	110	7.93	2.988	100 000	108 004
C	101	10.13	2.340	37 794	40 779
C	011	10.17	2.332	40 522	43 495
Pt	111	10.79	2.198	39 331	39 262
C	200	11.16	2.125	7425	9883
C	020	11.29	2.101	6775	8678
C	111	11.60	2.045	12 751	10 787
Pt	200	12.46	1.904	23 480	19 569
C	210	12.51	1.896	2136	1771
C	120	12.60	1.884	1225	1056
C	211	15.12	1.571	59 246	43 137
C	121	15.19	1.564	61 055	44 906
C	220	15.90	1.494	33 126	24 064
C	002	16.95	1.402	16 156	11 642

zation of the results. The abnormal dispersion for each chemical species was calculated using *CROMER* (Farrugia, 2002).

As the collected X-ray profiles show reflections from Pt, Re and NaCl, in addition to GeO_2 reflections, a multi-phase analysis was carried out with some profile parameters of the minor phases fixed to initial values or constrained to values of another phase. Lattice parameters were refined with initial values being refined prior to the Rietveld analyses.

The background was approximated by Legendre polynominals with ten parameters. A preferred-orientation correction was performed for the $CaCl_2$- and α-PbO_2-type phases, using the March–Dollase function (Dollase, 1986). The 'TCH' pseudo-Voigt function (Thompson *et al.*, 1987) with peak asymmetry described by two parameters with a physical basis, r_s and r_d (Finger *et al.*, 1994), was used as the peak profile function, in which the FWHM's (full width at half-maximum) of the Gaussian component (H_{KG}) and Lorentzian component (H_{KL}) are described, respectively, as

$$H_{KG} = \left[8 \ln 2 \left(U \tan^2 \theta + V \tan \theta + W\right)\right]^{1/2},$$
$$H_{KL} = (X + X_e \cos \varphi) \sec \theta + (Y + Y_e \cos \varphi) \tan \theta,$$

where U, V and W are the FWHM parameters from Caglioti *et al.* (1958), and X, X_e, Y and Y_e are the Lorentzian Scherrer broadening parameter, its anisotropy coefficient, the strain broadening parameter and its anisotropy coefficient (Larson & Von Dreele, 2000).

Since the FWHM parameters U, V and W are highly correlated to each other and the 2θ range measured is limited, V and W were only refined in the early stage of the least-squares cycles. All site occupancies were fixed to 1.0. The overall atomic displacement parameters were refined from initial values calculated at each temperature of the profile measurement (Lipson, 1967; Ibers *et al.*, 1968).

Initially, only the scale factor and background parameters were refined. The lattice constant and FWHM parameters

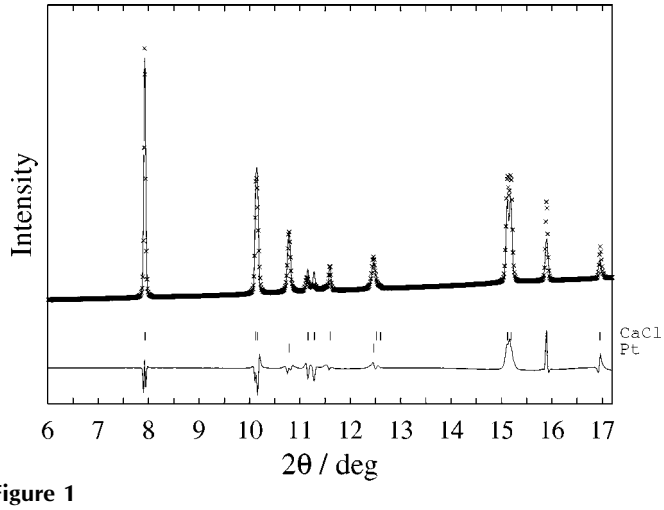

Figure 1
Fitted pattern of the Rietveld refinement of the $CaCl_2$-type phase. The crosses represent experimental points. The solid lines represent the calculated pattern and the difference curves. The short bars under the profiles show reflection positions for each phase.

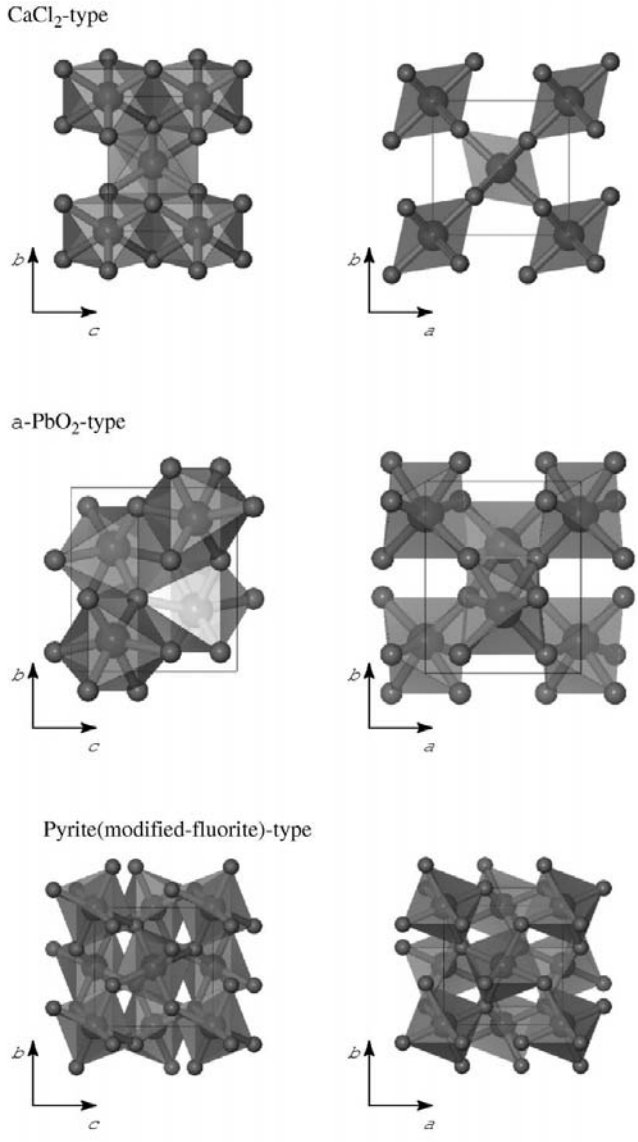

Figure 2
Refined structures of three GeO_2 phases. The polyhedra show GeO_8 octahedra.

Table 3
Structural data for the phases of GeO_2.

B_{iso} is the common parameter for Ge and O.

Phase	Space group	Cell constant (Å)	Site	Wyckoff symbol	Positions	B_{iso} (Å^2)	Pressure (GPa)
$CaCl_2$	*Pnnm*	*a* = 4.2499 (7)	Ge^{2+}	2(*a*)	0, 0, 0	0.35 (fixed)	30.1
	Z = 2	*b* = 4.2025 (7)	O^{2-}	4(*g*)	0.304 (5), 0.292 (6), 0		
		c = 2.8039 (4)					
α-PbO_2	*Pbcn*	*a* = 4.0519 (6)	Ge^{2+}	4(*c*)	0, 0.1687 (12), 0.25	2.9 (7)	70.7
	Z = 4	*b* = 5.0269 (6)	O^{2-}	8(*d*)	0.211 (5), 0.895 (3), 0.400 (2)		
		c = 4.5223 (6)					
Pyrite	$Pa\bar{3}$	*a* = 4.3365 (15)	Ge^{2+}	4(*a*)	0, 0, 0	0.446 (9)	108.0
	Z = 4		O^{2-}	8(*c*)	*x*, *x*, *x*, *x* = 0.3417 (16)		

were varied next. Then, other parameters, including the profile parameters and atomic coordinates, were refined. The resultant *R* factors, 2θ ranges and other refinement conditions for each refinement are also listed in Table 1.

3. Results and discussion

3.1. $CaCl_2$-type structure

The diffraction profile includes two phases: $CaCl_2$-type GeO_2 and platinum. A preferred-orientation correction was tried with different preferred-orientation vectors, with {111} resulting in the best fit (Fig. 1). The refined structure has octahedral chains linked by shared edges along the *c* axis (Fig. 2). The fitted peak positions are listed in Table 2. The refined atomic coordinates and selected bond lengths are listed in Tables 3 and 4, respectively. Since refinement of the overall isotropic atomic displacement parameter resulted in a negative value it was fixed to the initial value of 0.35 Å^2, which had been calculated for Ge at 300 K by approximation (Lipson, 1967; Ibers *et al.*, 1968).

The fitted result (Fig. 1) shows large residuals at the positions of the (211), (121) and (220) reflections of GeO_2. These residuals could not be decreased even by the correction of the preferred orientation. The reason for this uncorrectable preferred orientation is unclear. This misfit decreases the reliability of the refined atomic coordinates.

Haines *et al.* (2000) studied the phase transformation of rutile-type GeO_2 to $CaCl_2$-type GeO_2 in a pressure range from ambient to 36 GPa. The Rietveld refinements using high-pressure XRD data demonstrated that the GeO_6 octahedron elongated along the axial Ge—O bond at ambient pressure. However, at higher pressure it deformed into a flattened shape as a result of the larger compression of the two axial bonds of the octahedron than of the four equatorial bonds. The transformation from rutile-type to $CaCl_2$-type was observed at 25 GPa, during the flattening of the octahedron.

In the present work, at 30 GPa and 300 K, the octahedron has axial and equatorial distances of 1.78 (2) and 1.85 (2) Å, respectively. Comparing these distances with those described by Haines *et al.* (2000) at a pressure of 29 GPa (axial and equatorial distances of 1.808 and 1.862 Å), the present result proposes a more anisotropic octahedron, but the misfit between the calculated and the observed profiles reduces the reliability of this comparison.

3.2. α-PbO_2-type structure

3.2.1. Refinement as the ordered phase. The diffraction profile was analyzed as a three-phase system containing α-PbO_2-type GeO_2, NaCl and platinum (Fig. 3). No correction for the preferred orientation was made. The refinement was carried out successfully (R_{wp} = 0.77). The fitted peak positions are listed in Table 5. The overall isotropic atomic displacement parameter B_{iso} was refined starting from an initial value of 2.4 Å^2, which was calculated for Ge at 2110 K in the same way as in the analysis of the $CaCl_2$-type. The refinement gave 2.9 (7) Å^2 for B_{iso}. An attempt at refinement with fixed anisotropy coefficients $X_e = Y_e = 0$ resulted in an unusually large B_{iso} and the atomic coordinates were significantly influenced by the large B_{iso}. To avoid this difficulty in further analysis, X_e and Y_e were refined together with the other variable peak profile parameters, *U*, *X*, *Y*, r_s and r_d. This refinement gave a reasonable value of B_{iso}, as listed in Table 3.

The refined atomic coordinates and selected bond lengths are listed in Tables 3 and 4, respectively. The refined crystal structure is illustrated in Fig. 2. It shows zigzag octahedral chains along the *c* axis (Fig. 4*a*). Two of the six Ge—O distances are elongated compared with the other four bond distances (Table 4). The Ge atom is displaced from the center of the octahedron. This deformation of the octahedron was also indicated by the *ab initio* calculations of Łodziana *et al.* (2001), Table 4.

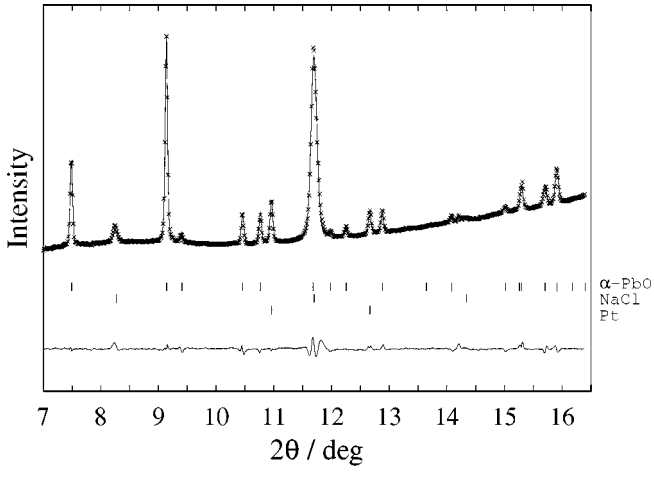

Figure 3
Fitted pattern of the Rietveld refinement of the α-PbO_2-type phase. The observed, calculated and difference curves are represented as in Fig. 1. The short bars under the profiles show reflection positions for each phase.

Table 4
Bond distances of octahedral sites in refined GeO_2 structures.

		Łodziana *et al.* (2001)		This work		
Phase		Distance (Å)	Pressure (GPa)	Distance (Å)	Pressure (GPa)	Bond multiplicity
$CaCl_2$-type	Ge—O	1.814	30	1.78 (2)	30.1	×2
		1.827		1.85 (2)		×4
α-PbO_2-type	Ge—O	1.860	40	1.75 (2)	70.7	×2
		1.814		1.83 (2)		×2
		1.772		1.77 (2)		×2
Pyrite-type	Ge—O	1.800	70	1.772 (6)	108.0	×6
	O—O	2.352		2.310 (9)		×6
		2.725		2.687 (9)		×6
	Ge—O†	2.622		2.567 (7)		×2
	O—O†	2.352		2.310 (9)		×6

† Interpolyhedral atomic distances (as illustrated in Fig. 7).

A unit cell of the α-PbO_2 structure has two occupied and two vacant octahedral sites (Fig. 4*a*). In this structure the Ge site can be disordered to obtain the defect-NiAs structure with a cation site occupancy of 0.5 (Fig. 4*b*).

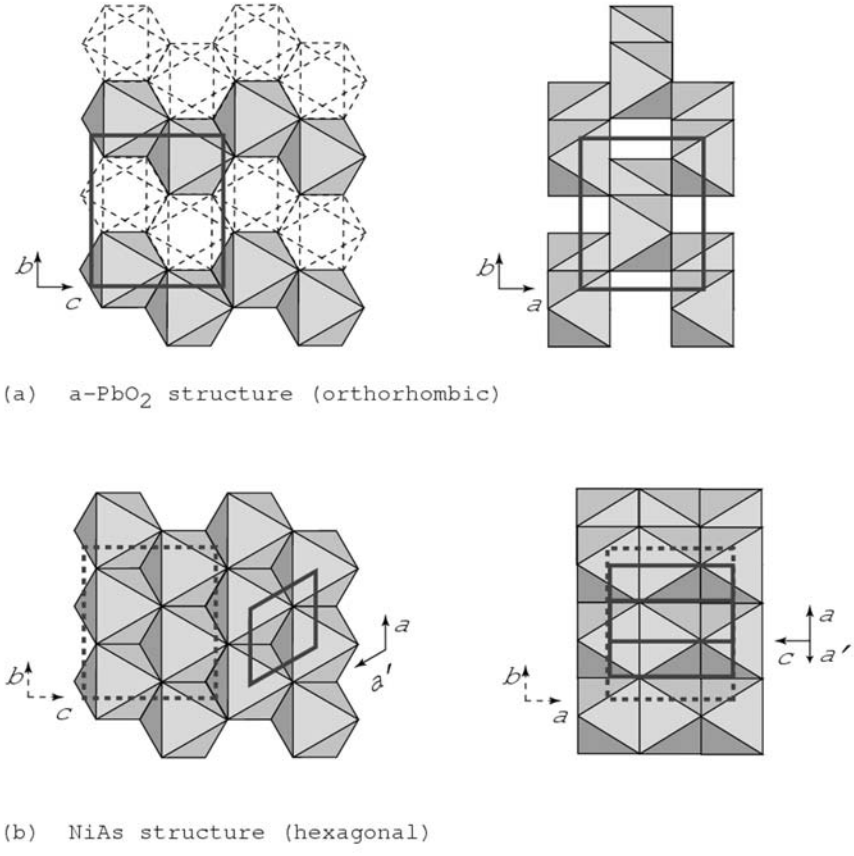

Figure 4
Order–disorder relationship between (*a*) the α-PbO_2 structure (ordered phase) and (*b*) the defect-NiAs structure (disordered phase). The defect-NiAs structure has a half-site occupancy for Ge. The boxes give the unit cells.

3.2.2. Order–disorder of the Ge site. The same profile was analyzed assuming a defect-NiAs structure, in order to check the possibility of disordering of the Ge site. A GeO_2 high-pressure phase with a defect-NiAs structure was reported by Liu *et al.* (1978) and was also termed the 'Fe_2N structure'. The defect-NiAs structure is described by the hexagonal system and space group $P6_3/mmc$. Prior to Liu *et al.* (1978), a ζ-Fe_2N structure had been determined by Jack (1948) as orthorhombic, *Pbcn*. Although he did not describe a space group and positions for all the atoms in the unit cell, the atomic coordinates can be translated so that an inversion centre is located at the origin. This translation gives the space group *Pbcn* and only two atomic coordinates are required in order to describe the whole ζ-Fe_2N structure. More recently, Rechenbach & Jacobs (1996) refined the ζ-Fe_2N structure with a space group *Pbcn*, confirming the analysis of Jack (1948). The ζ-Fe_2N structure has an ordered N site like the α-PbO_2 structure and is equivalent to the α-PbO_2 structure.

This historical usage of the term 'Fe_2N structure' may result in confusion. To avoid this, in this paper we use the term 'α-PbO_2 structure' for the ordered phase and 'defect-NiAs structure' for the disordered phase.

The Rietveld analysis, assuming a defect-NiAs structure with half occupancy, gave a remarkably large residual, as shown in Fig. 5. It shows that the disordering resulted in extinctions of some of the reflections, causing the large residual. By comparing the fitting results of the ordered and the disordered structures, it is concluded that the Ge site is completely ordered.

3.3. Pyrite-type (modified-fluorite-type) structure

The diffraction profile was analyzed as a three-phase system containing pyrite-type (modified-fluorite-type) GeO_2, rhenium and platinum. No correction for the preferred orientation was made. The overall isotropic atomic displacement parameter was refined starting from the initial value of 0.35 $Å^2$ calculated

Table 5
Observed and calculated intensities, and the positions of the diffraction peaks for the α-PbO_2-type structure.

Phase	*hkl*	2θ (°)	*d* (Å)	I_{obs}	I_{calc}
AP	110	7.49	3.155	20 333	20 280
N	100	8.27	2.860	5787	5335
AP	111	9.14	2.587	47 754	48 181
AP	020	9.41	2.513	2689	2673
AP	002	10.46	2.261	8150	8821
AP	021	10.77	2.197	7468	8065
Pt	111	10.96	2.158	11 892	12 389
AP	200	11.68	2.026	3521	3449
N	110	11.70	2.022	100 000	99 003
AP	102	11.98	1.974	2063	2057
AP	121	12.25	1.931	1751	2529
Pt	200	12.66	1.869	5771	6164
AP	112	12.88	1.838	5148	5179
AP	211	13.64	1.735	463	146
AP	022	14.09	1.681	3218	2601
N	111	14.34	1.651	830	869
AP	220	15.02	1.577	2603	2407
AP	122	15.26	1.553	84	80
AP	130	15.30	1.548	6680	6633
AP	202	15.70	1.509	6830	6664

for Ge at a temperature of 300 K in the same manner as the case of the $CaCl_2$-type structure. The profile parameters U, X, X_e, Y, Y_e, r_s and r_d were refined. The refinement gave an acceptable value of B_{iso}, as listed in Table 3.

The fitting result shows a small residual (Fig. 6). The fitted peak positions are listed in Table 6. The refined structure shows GeO_6 octahedra sharing all apices with adjacent octahedra and without edge-sharing (Fig. 2). This structural feature results in a high density. The GeO_6 octahedron is symmetric and the cation is placed at the center of the octahedron. The GeO bond length is 1.772 (6) Å. This is a little shorter than that calculated by Łodziana *et al.* (2001) at 70 GPa and 0 K (Table 4). However, considering the conditions in the present study, 108 GPa and 300 K, these two values are in agreement with each other. The atomic coordinates of this study and Łodziana *et al.* (2001) are very similar

Table 6
Observed and calculated intensities, and the positions of the diffraction peaks for the pyrite-type (modified fluorite-type) structure.

Phase	*hkl*	2θ (°)	*d* (Å)	I_{obs}	I_{calc}
py	111	9.46	2.504	100 000	99 629
Re	100	10.51	2.254	8402	8424
py	200	10.93	2.168	42 039	41 585
Pt	111	11.26	2.106	21 224	21 038
Re	002	11.39	2.081	284	287
Re	101	11.96	1.982	6719	6757
py	210	12.22	1.939	8044	8169
Pt	200	13.00	1.823	3434	3810
py	211	13.395	1.770	–	3374

[0.3417 (16) and 0.3473, respectively]. The difference in the lattice constants (4.4066 Å at 70 GPa by Łodziana *et al.*, 2001, and 4.3365 Å at 108 GPa in the present work) implies a pressure-dependent compressibility.

In the pyrite-type (modified-fluorite-type) structure the Ge site is described as being six-coordinate. Including two additional anions, the Ge site is eightfold-coordinated and of rhombohedral shape. The rhombohedral angle, α, of this polyhedron can be related to the anion coordinate x (Haines & Léger, 1997). In an ideal pyrite structure, the oxygen x coordinate is 0.38, which leads to $\alpha = 60^\circ$ and a regular octahedron. Decreasing the x value results in an increase in the α angle, which causes a transformation of the rhombohedron to a cubic shape. For $x = 0.25$, the polyhedron becomes an ideal cube of cations and the whole structure is equal to an ideal fluorite structure. Fig. 7 illustrates this transformation of the GeO_8 polyhedron from a rhombohedron to a cube, which would be expected to appear in the compression process of GeO_2 minerals.

Haines & Léger (1997) studied the pyrite-type (modified-fluorite-type) SnO_2, in which x decreases with increasing pressure. They reported $x = 0.347$ (1) at 48 GPa, which is close to the present result for GeO_2, $x = 0.3417$ (16) at 108 GPa,

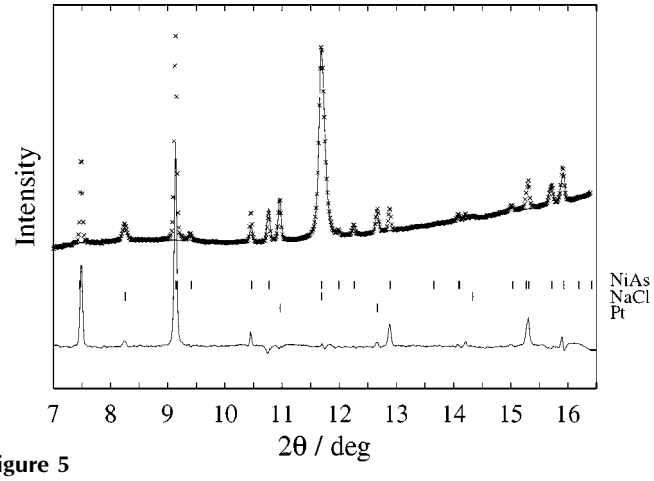

Figure 5
Fitted pattern of the Rietveld refinement of the same profile as in Fig. 3, assuming a defect-NiAs structure (disordered phase). The observed, calculated and difference curves are represented as in Fig. 1. The short bars under the profiles show the reflection positions for each phase.

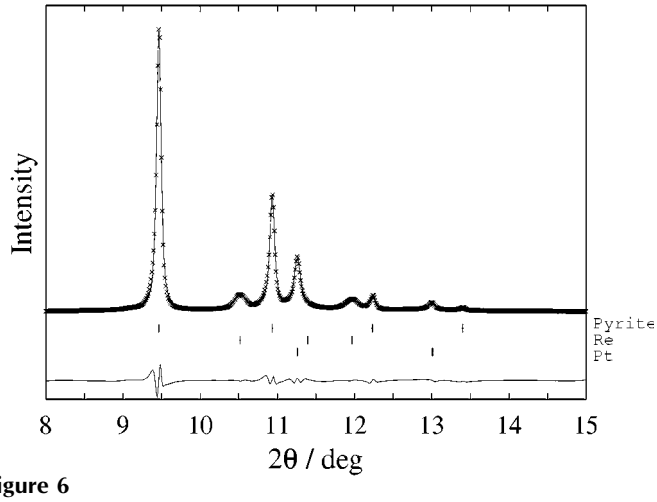

Figure 6
Fitted pattern of the Rietveld refinement of the pyrite-type (modified fluorite-type) phase. The observed, calculated and difference curves are represented as in Fig. 1. The short bars under the profiles show the reflection positions for each phase.

Table 7
Pressures of the phase transitions for GeO_2 and SiO_2 polymorphs in previous theoretical and experimental works.

GeO_2	Reference	Rutile-type ($P4_2/mnm$) (GPa)	$CaCl_2$-type ($Pnnm$) (GPa)	α-PbO_2-type ($Pbcn$) (GPa)	Pyrite-type ($Pa3$)	Method
	Łodziana *et al.* (2001)	~19	36		65.5	*Ab initio* calc.
	Ono *et al.* (2003*b*)	19	30		59	*Ab initio* calc.
	Haines *et al.* (2000)	~25				Exp.
	Ono *et al.* (2003*b*)		33			Exp.
SiO_2						
	Karki *et al.* (1997)	47	98		226	*Ab initio* calc.
	Teter *et al.* (1998)	55	85		205	*Ab initio* calc.
	Andrault (1998)	54		Exp.		
	Ono, Hirose, Murakami & Isshiki (2002)	55		Exp.		

leading to $\alpha = 70.3$ and 71.1°. Assuming that a higher pressure could induce a transformation to the ideal fluorite structure ($x = 0.25$) with increasing coordination number of the cation from six to eight, the present result is regarded as being in a transitional state between the ideal pyrite structure and the ideal fluorite structure (Fig. 7). Further compression is expected until the GeO_8 rhombohedron might be deformed into a cube which is characteristic of the ideal fluorite structure.

3.4. Theoretical and experimental sequences of the phase transition

Two *ab initio* studies on the phase transition of GeO_2 (Łodziana *et al.*, 2001; Ono, Hirose, Murakami & Isshiki, 2002) gave the same theoretical sequence, which is rutile-type ⇒ $CaCl_2$-type ⇒ α-PbO_2-type ⇒ pyrite-type (modified-fluorite-type). A series of experimental studies on the high-pressure phase of GeO_2 (Ono, Hirose, Nishiyama & Isshiki, 2002; Ono, Hirose, Issiki *et al.*, 2003; Ono, Hirose, Murakami & Isshiki, 2002) gave a transition sequence in agreement with the theoretical one. Experimental values of transition pressure show good agreement with the theoretical values, as shown in Table 7.

GeO_2 is known to be a low-pressure analog of SiO_2, which also has the same transition sequence as GeO_2. Two theoretical studies on the high-pressure phase of SiO_2 (Karki *et al.*, 1997; Teter *et al.*, 1998) are in a good agreement each other.

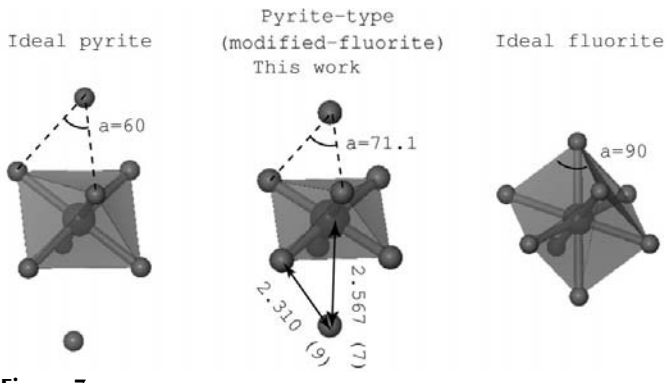

Figure 7
Structural relationships of ideal pyrite, ideal fluorite and the refined structure of the pyrite-type (modified fluorite-type) phase.

Although Karki *et al.* (1997) concluded that a *Pnc*2 structure is stable instead of the α-PbO_2-type, it was confirmed that the *Pnc*2 structure can be described using the higher symmetry *Pbcn* and completely coincides with the α-PbO_2-type structure (Teter *et al.*, 1998). Consequently, these two studies gave the same sequence.

Previous experimental studies searched only the lower part of the transition sequence for SiO_2 (up to *ca* 100 GPa). A structural deformation in the higher part of the sequence (post-$CaCl_2$-type phase transition) can be predicted by the GeO_2 studies. The $CaCl_2$-type structure undergoes a phase transition to the α-PbO_2-type structure to make a 2×2 zigzag arrangement of SiO_6 octahedra with edge-sharing. At a pressure of *ca* 200 GPa, the α-PbO_2-type structure transforms into the pyrite-type or the modified fluorite-type structure, in which the Si—O distances along the long axis of the SiO_8 rhombohedron will be shortened during further compression. The fluorite-type structure will finally appear if further compression could be continued until the SiO_8 rhombohedron deformed into a cube.

4. Conclusions

The crystal structures of the GeO_2 polymorphs were refined with the Rietveld method, using synchrotron radiation data collected *in situ* at high pressure. The refined GeO_2 polymorphs are the $CaCl_2$-type, α-PbO_2-type and pyrite-type (modified-fluorite-type) structures. The refinements were successful, except for the $CaCl_2$-type, which gave a significant residual of the profile fitting for three reflections which could not have been improved even with adopting the preferred-orientation correction. The refinements of the α-PbO_2-type and pyrite-type (modified fluorite-type) structures gave atomic positions with sufficient quality to discuss their structural features. The structural characteristics are in agreement with the *ab initio* calculations of Łodziana *et al.* (2001). Cation disordering of the α-PbO_2-type, which leads to the defect-NiAs structure, was tested, but no evidence of Ge disordering was found. The pyrite-type structure was revealed to be on a path of compression from the ideal pyrite-type structure to the ideal fluorite-type structure.

These structural refinement results provide important silica analogs, since the high-pressure polymorphs of silica are also expected to have the same sequence as GeO_2. Considering experimental and theoretical studies on the high-pressure phase transitions of SiO_2 and GeO_2, the phase transition of SiO_2, similar to that of GeO_2, will take place based on the same mechanism of structural deformation as GeO_2, but at higher pressures.

This study provides structural data of GeO_2 high-pressure polymorphs and supports the descriptions of the GeO_2 high-pressure phase based on the experimental studies (Ono, Hirose, Nishiyama & Isshiki, 2002; Ono *et al.*, 2003*a*,*b*).

We thank M. Isshiki and Y. Ohishi for experimental assistance. The synchrotron radiation experiments were performed at the SPring-8 with the approval of the Japan Synchrotron Radiation Research Institute (JASRI) (Proposal No. 2002 A0106-ND2-np and 2002B0162-ND2-np).

References

Andrault, D., Fiquet, G., Guyot, F. & Hanfland, M. (1998). *Science*, **282**, 720–724.
Baur, W. H. & Khan, A. A. (1971). *Acta Cryst.* B**27**, 2133–2139.
Cagliotti, G., Pauletti, A. & Ricci, F. P. (1958). *Nucl. Instrum. Methods*, **3**, 223.
Dilanian, R. A. & Izumi, F. (2002). *VENUS*, http://homepage.-mac.com/fujioizumi/visualization/VENUS.tbz.
Dollase, W. A. (1986). *J. Appl. Cryst.* **19**, 267–272.
Dubrovinsky, L. S., Dubrovinskaia, N. A., Saxena, S. K., Tutti, F., Rekhi, S., Le Bihan, T., Shen, G. & Hu, J. (2001). *Chem. Phys. Lett.* **333**, 264–270.
Dubrovinsky, L. S., Saxena, S. K., Lazor, P., Ahuja, R., Eriksson, O., Wills, J. M. & Johansson, B. (1997). *Nature*, **388**, 362–365.
Farrugia, L. F. (2002). *CROMER for Windows*, http://ccp14.minerals.csiro.au/ccp/web-mirrors/farrugia/~louis/software/cromer.
Finger, L. W., Cox, D. E. & Jephcoat, A. P. (1994). *J. Appl. Cryst.* **27**, 892–900.
Haines, J. & Léger, J. (1997). *Phys. Rev. B*, **55**, 11144–11154.
Haines, J., Léger, J., Chateau, C. & Pereira, A. S. (2000). *Phys. Chem. Miner.* **27**, 575–582.
Haines, J., Léger, J., Gorelli, F. & Hanfland, M. (2001). *Phys. Rev. Lett.* **87**, 155503–155506.
Hazen, R. & Finger, L. W. (1981). *J. Phys. Chem. Solids*, **42**, 143–151.
Holmes, N. C., Moriarty, J. A., Gathers, G. R. & Nellis, W. J. (1989). *J. Appl. Phys.* **66**, 2962–2967.
Ibers, J. A., Templeton, D. H., Vainshtein, B. K., Bacon, G. E. & Lonsdale, K. (1968). *International Tables for X-ray Crystallography*, edited by K. Lonsdale, Vol. III, pp. 233–244. Birmingham: Kynoch Press.
Izumi, F. & Ikeda, T. (2000). *Mater. Sci. Forum*, **198**, 321–324.
Jack, K. H. (1948). *Proc. R. Soc. London Ser. A*, **195**, 34–40.
Jackson, I. (1976). *Phys. Earth Planet. Inter.* **13**, 218–231.
Karki, B. B., Warren, M. C., Stixrude, L., Ackland, G. J. & Crain, J. (1997). *Phys. Rev. B*, **55**, 3465–3471.
Kingma, K. J., Cohen, R. E., Hemley, R. J. & Mao, H. K. (1995). *Nature*, **374**, 243–245.
Kingma, K. J., Mao, H. K. & Hemley, R. J. (1996). *High Press. Res.* **14**, 363–374.
Liebermann, R. C. (1973). *Phys. Earth Planet. Inter.* **7**, 461–465.
Lipson, H. (1967). *International Tables for X-ray Crystallography*, edited by J. S. Kasper & K. Lonsdale, Vol. II, pp. 241–265. Birmingham: Kynoch Press.
Larson, A. C. & Von Dreele, R. B. (2000). *General Structure Analysis System (GSAS)*. Los Alamos National Laboratory Report LAUR 86–748. Los Alamos, New Mexico.
Liu, L., Bassett, W. A. & Sharry, J. (1978). *J. Geophys. Res.* **83**, 2301–2305.
Łodziana, Z., Parlinski, K. & Hafner, J. (2001). *Phys. Rev. B*, **63**, 134106–134112.
Navrotsky, A. (1971). *J. Inorg. Nucl. Chem.* **33**, 1119–1124.
Ono, S., Hirose, K., Isshiki, M., Mibe, K. & Saito, Y. (2002). *Phys. Chem. Miner.* **29**, 527–531.
Ono, S., Hirose, K., Murakami, M. & Isshiki, M. (2002). *Earth Planet. Sci. Lett.* **197**, 187–192.
Ono, S., Hirose, K., Nishiyama, N. & Isshiki, M. (2002). *Am. Mineral.* **87**, 99–102.
Ono, S., Tsuchiya, T., Hirose, K. & Ohishi, Y. (2003*a*). *Phys. Rev. B*, **68**, 14103–14107.
Ono, S., Tsuchiya, T., Hirose, K. & Ohishi, Y. (2003*b*). *Phys. Rev. B*, **68**, 134108–134114.
Rao, K. V. K., Naidu, S. V. N. & Iyengar, L. (1968). *J. Am. Ceram. Soc.* **51**, 467–468.
Rechenbach, D. & Jacobs, H. (1996). *J. Alloys Compds*, **235**, 15–22.
Shen, G., Rivers, M. L., Wang, Y. & Sutton, R. (2001). *Rev. Sci. Instrum.* **72**, 1273–1282.
Teter, D. M., Hemley, R. J., Kresse, G. & Hafner, J. (1998). *Phys. Rev. Lett.* **80**, 2145–2148.
Thompson, P., Cox, D. E. & Hastings, J. B. (1987). *J. Appl. Cryst.* **20**, 79–83.
Toraya, H. (1990). *J. Appl. Cryst.* **23**, 485–489.
Tsuchiya, T. & Kawamura, K. (2002). *Phys. Rev. B*, **66**, 94115–94119.